Global Biogeochemical Cycles

RESEARCH ARTICLE
10.1029/2022GB007596

Special Section:
Southern Ocean and Climate: Biogeochemical and Physical Fluxes and Processes

Fingerprint of Climate Change on Southern Ocean Carbon Storage

R. M. Wright[1], C. Le Quéré[1], N. Mayot[1], A. Olsen[2,3], and D. C. E. Bakker[1]

[1]Centre for Ocean and Atmospheric Sciences, School of Environmental Sciences, University of East Anglia, Norwich, UK, [2]Geophysical Institute, University of Bergen, Bergen, Norway, [3]Bjerknes Centre for Climate Research, Bergen, Norway

Key Points:

- The effect of decadal climate variability on dissolved inorganic carbon (DIC) in the Southern Ocean is nearly as large as that of atmospheric CO_2
- Climatic drivers cause a distinct fingerprint on the change in DIC concentration in the Southern Ocean interior
- This fingerprint could serve to detect future trends in Southern Ocean carbon storage

Correspondence to:
R. M. Wright,
rebecca.wright@uea.ac.uk

Citation:
Wright, R. M., Le Quéré, C., Mayot, N., Olsen, A., & Bakker, D. C. E. (2023). Fingerprint of climate change on Southern Ocean carbon storage. *Global Biogeochemical Cycles*, *37*, e2022GB007596. https://doi.org/10.1029/2022GB007596

Received 30 SEP 2022
Accepted 27 MAR 2023

Author Contributions:
Conceptualization: R. M. Wright, C. Le Quéré
Formal analysis: R. M. Wright, C. Le Quéré
Funding acquisition: C. Le Quéré
Investigation: R. M. Wright
Methodology: R. M. Wright, C. Le Quéré, N. Mayot, A. Olsen
Supervision: C. Le Quéré
Validation: R. M. Wright
Visualization: R. M. Wright
Writing – original draft: R. M. Wright
Writing – review & editing: R. M. Wright, C. Le Quéré, N. Mayot, A. Olsen, D. C. E. Bakker

Abstract The Southern Ocean plays a critical role in the uptake, transport, and storage of carbon by the global oceans. It is the ocean's largest sink of CO_2, yet it is also among the regions with the lowest storage of anthropogenic carbon. This behavior results from a unique combination of high winds driving the upwelling of deep waters and the subduction and northward transport of surface carbon. Here we isolate the direct effect of increasing anthropogenic CO_2 in the atmosphere from the indirect effect of climate variability and climate change on the reorganization of carbon in the Southern Ocean interior using a combination of modeling and observations. We show that the effect of climate variability and climate change on the storage of carbon in the Southern Ocean is nearly as large as the effect of anthropogenic CO_2 during the period 1998–2018 compared with the climatology around the year 1995. We identify a distinct climate fingerprint in dissolved inorganic carbon (DIC), with elevated DIC concentration in the ocean at 300–600 m that reinforces the anthropogenic CO_2 signal, and reduced DIC concentration in the ocean around 2,000 m that offsets the anthropogenic CO_2 signal. The fingerprint is strongest at lower latitudes (30°–55°S). This fingerprint could serve to monitor the highly uncertain evolution of carbon within this critical ocean basin, and better identify its drivers.

1. Introduction

The Southern Ocean is one of the world's most important regions for the carbon cycle and the regulation of atmospheric CO_2 concentration, accounting for around a third of the global oceanic uptake of anthropogenic CO_2 resulting from human activities (Friedlingstein et al., 2021). Paradoxically, the Southern Ocean is also among the ocean basins with the lowest storage of anthropogenic carbon (Gruber, Clement, et al., 2019), especially considering its high uptake. This high uptake/storage ratio is caused by a unique combination of intense circumpolar winds driving the upwelling of deep waters that have not been in contact with the atmosphere for centuries, and the vigorous subduction and northward transport of surface carbon within the Antarctic Intermediate Water and Subantarctic Mode Water.

Atmospheric conditions over the Southern Ocean have changed in recent decades, with winds strengthening in response to the depletion of stratospheric ozone reinforced by climate change (Fyfe & Saenko, 2006; Thompson & Solomon, 2002; Thompson et al., 2011). While the strengthening of the winds is clear over multiple decades, the effect on the vertical transport of water masses, and hence on the reorganization of carbon within the ocean, is highly uncertain (Meredith et al., 2019). The difficulty comes from quantifying the relative effect of enhanced upwelling in response to the intensification of the winds, and the opposing effect of the intensification of eddies that results from the upwelling-driven steepening of isopycnals (Morrison et al., 2021). In addition, changes in sea-ice and buoyancy fluxes (precipitation and heat) are also altering vertical mixing and the transport of carbon, complicating the picture further. The latest assessment by the Intergovernmental Panel on Climate Change reports no consensus on the combined effects of these Earth System changes on the physical transport of water masses in the Southern Ocean due to conflicting evidence and poor model representations of key processes (Fox-Kemper et al., 2021). Uncertainties in physical changes translate directly into uncertainties in carbon changes, with carbon changes further compounded by potential changes in biological processes that are largely unknown. Wind variability also complexifies the detection of any longer-term trends.

Estimates based on carbon observations in the atmosphere and in the surface ocean have been used to infer changes and variability in recent decades, with evidence of periods of "saturation" (Le Quéré et al., 2007) followed by "reinvigoration" (Landschützer et al., 2015) of the Southern Ocean CO_2 sink. These decadal swings can only be explained by the large variability of the Southern Ocean in response to climatic change and/or

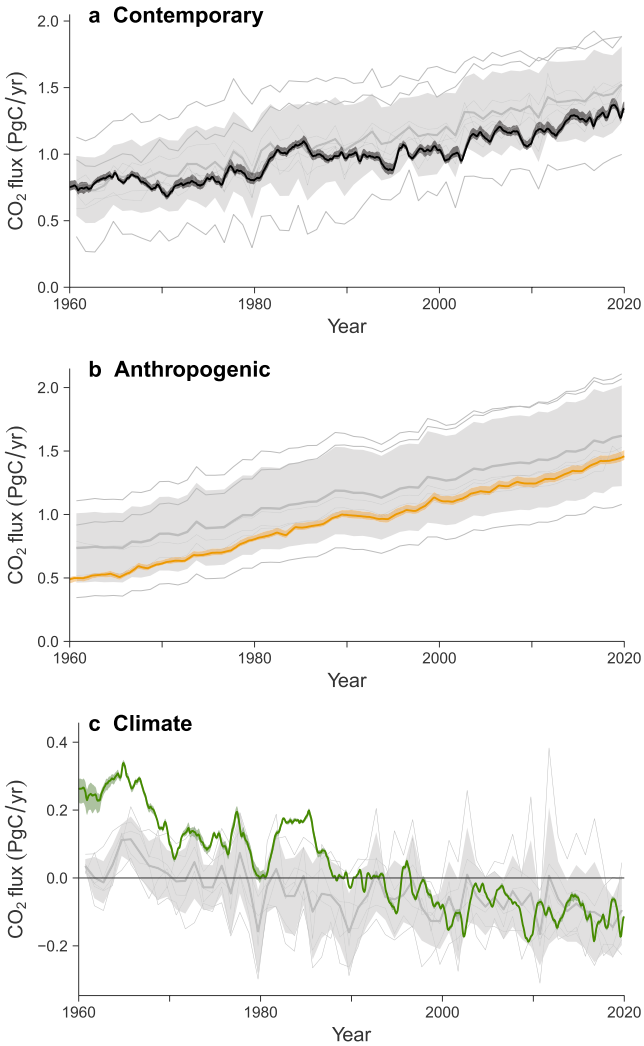

Figure 1. Southern Ocean CO_2 flux in Global Ocean Biogeochemical Models for (a) contemporary, (b) anthropogenic, and (c) climate carbon (PgC/yr). The CO_2 flux is positive from the atmosphere into the ocean. The Southern Ocean is defined as south of 35°S. The monthly NEMO-PlankTOM12 three-member ensemble mean used in this study is shown by the colored lines with the ensemble min/max (colored shading). The yearly Global Carbon Budget multi-model mean is shown by the thick gray lines with the ±1 standard deviation (gray shading). Each individual Global Carbon Budget model is shown by the thin gray lines. Carbon is partitioned into contemporary (from increasing atmospheric CO_2, climate change, and climate variability), anthropogenic (from increasing atmospheric CO_2 only), and climate (from climate change and climate variability, calculated as the difference between contemporary and anthropogenic carbon).

variability, including that related to ozone depletion (Thompson et al., 2011). Estimates using ocean carbon models also show a response of the Southern Ocean CO_2 sink to climate variability, but models overwhelmingly produce a small climate response that is almost entirely hidden by the large response to the rise in anthropogenic CO_2 (DeVries et al., 2019). Some of the model-data discrepancies could be explained by the paucity of observations, as differences are largest in locations with no observations (Hauck et al., 2020), and data gaps can lead to about 30% excessive variability in data products (Gloege et al., 2021). This limited evidence and quantitative understanding of the underlying processes means we currently have very little confidence in recent changes in the Southern Ocean carbon storage, and little insight into their likely persistence in the future.

From a process perspective, it would be expected that anthropogenic carbon increases the most near the surface everywhere, as it penetrates the ocean from the atmosphere, with more increase below the surface in the subduction regions and less increase below the surface in the upwelling regions. Conversely, it would be expected that natural carbon will show stronger changes in the upwelling regions than elsewhere in the ocean.

Here we take advantage of the high ratio between the climatic and anthropogenic drivers of changes in carbon on decadal timescales within the Southern Ocean to identify the combined effect of climate-related changes relative to the direct anthropogenic changes on the reorganization of carbon in the Southern Ocean, and the implications for the future. We identify a fingerprint for these two processes that could serve to monitor the evolution of carbon within this critical ocean basin.

We use a combination of modeling and observations to quantify the relative contribution of different drivers to the storage of DIC in the Southern Ocean. We use observations from the Global Ocean Data Analysis Project (GLODAP), a regularly updated synthesis of ocean surface and interior biogeochemical data (Olsen et al., 2020) and use NEMO-PlankTOM12, a state-of-the-art Global Ocean Biogeochemical Model (GOBM) used in the Global Carbon Budget (GCB, Friedlingstein et al., 2021). We partition contemporary DIC into its component parts of anthropogenic and climate carbon (Figure 1) and calculate the change in DIC for each during the period 1998–2018 relative to climatology centered around the year 1995, providing a fingerprint in DIC. We use the model to directly attribute this climate fingerprint to various climatic drivers. Understanding how the Southern Ocean sink responds to climate change and climate variability is key to understanding how the global ocean sink will evolve over the coming decades.

2. Methods

2.1. The NEMO-PlankTOM12 Model Simulations

2.1.1. Model Description

PlankTOM12 is a global ocean biogeochemistry model with full marine cycles of key elements carbon, oxygen, phosphorus, and silicon, and simplified cycles of nitrogen and iron. PlankTOM12 simulates plankton ecosystem processes and their interactions with the environment through the representation of 12 plankton functional types (PTFs). Spatial variability within PFTs is represented through parameter-dependence on environmental conditions including temperature, nutrients, light, and food availability. PlankTOM12 represents sinking processes through the aggregation and disaggregation of organic material into two particles of different size classes: a small particle that sinks at a constant 3 m per day, and a large particle that sinks at a variable speed that depends on the ballasting of minerals

Table 1
NEMO-PlankTOM12 Model Simulations and the Formulations Used to Isolate Drivers of Changes in Carbon

	Drift	Pre-industrial carbon	Atmospheric CO_2	Variable climate	Variable wind speed	Variable wind stress	Variable buoyancy
Simulation							
sim[1]	Y	Y					
sim[2]	Y	Y	Y				
sim[3]	Y	Y	Y	Y	Y	Y	Y
sim[4]	Y	Y	Y	Y		Y	
sim[5]	Y	Y	Y	Y	Y		
Formulation							
Contemporary (Equation 1)			Y	Y	Y	Y	Y
Anthropogenic (Equation 2)			Y				
Climate (Equation 3)				Y	Y	Y	Y
Wind speed (Equation 4)					Y		
Wind stress (Equation 5)						Y	
Buoyancy (Equation 6)							Y

Note. Each sim[1–5] was run with each of the three spin-up years, 1959, 1990, and 2013, and the 3-member ensemble average is presented in the text. Variable wind stress influences ocean circulation, while variable wind speed influences the CO_2 gas exchange.

(Buitenhuis et al., 2013). For a full description of PlankTOM biogeochemistry, see Wright et al. (2021) and Le Quéré et al. (2016).

PlankTOM12 is coupled online to the global ocean general circulation model Nucleus for European Modelling of the Ocean version 3.6 (NEMO v3.6-ORCA2). We used the global configuration with a horizontal resolution of 2° longitude by a resolution of 0.3°–1.5° latitude using a tripolar orthogonal grid. The vertical resolution is 10 m for the top 100 m; below 100 m, the resolution incrementally decreases with each subsequent depth level, reaching a resolution of 500 m at 5 km depth, with a total of 31 vertical z levels (Madec, 2013). The ocean is described as a fluid using the Navier–Stokes equations and a nonlinear equation of state (Madec, 2013). NEMO v3.6 explicitly calculates vertical mixing at all depths using a turbulent kinetic energy model and sub-grid eddy-induced mixing. The model is interactively coupled to a thermodynamic sea-ice model (LIM version 2, Timmermann et al., 2005).

2.1.2. Main Simulations

The NEMO-PlankTOM12 simulations for this study were developed from the published simulations in the GCB 2021 (Friedlingstein et al., 2021), with the changes outlined below. Three simulations were devised in order to isolate the effects of climate change and climate variability from that of anthropogenic CO_2 (Table 1; sim[1], sim[2], and sim[3]). sim[1] is designed as a control simulation that will be used to remove any residual model drift. It is forced by atmospheric CO_2 of 278 ppm, including pre-industrial carbon in the initial conditions. The forcing fields are constant, which is achieved by looping over the daily fields for 1 year, therefore including no trends or variability in climate. sim[2] is designed to capture the effect of increasing anthropogenic CO_2 in the atmosphere. It is forced by the global observed monthly mean atmospheric CO_2, with the forcing fields looping over 1 year as in sim[1], therefore including trends and variability in anthropogenic CO_2 alone. sim[3] is the best estimate of the contemporary CO_2 fluxes. It is forced by the global observed monthly mean atmospheric CO_2 and by the daily forcing fields of the year of the simulation, therefore including trends and variability in both anthropogenic CO_2 and climate.

Each simulation is repeated three times with a different forcing year for looping and spin-up. The forcing years are 1959, 1990, and 2013, selected as "representative" years with no strong El Niño/La Niña present. Year 1990 is also the year used in the GCB GOBM ensemble for looping and spin-up (Friedlingstein et al., 2021). sim[1] is run three times from 1750 to 2020, each repeating one of the three forcing years, keeping atmospheric CO_2 constant at 278 ppm. sim[2] is run three times from 1750 to 2020, each repeating one of the three forcing years, with observed increasing atmospheric CO_2. sim[3] is initialized three times, from each of the three sim[2] simulations in 1947, and then each is run until 2020 with daily observed forcing fields and observed increasing atmospheric CO_2.

For sim^1, sim^2, and sim^3, the three members (forcing years 1959, 1990, and 2013) are averaged. These 3-member averages are then combined in a variety of ways to isolate drivers of trends in ocean DIC;

$$DIC_{CO}^{mod} = sim^3 - sim^1 \quad (1)$$

$$DIC_{AN}^{mod} = sim^2 - sim^1 \quad (2)$$

$$DIC_{CL}^{mod} = sim^3 - sim^2 \quad (3)$$

Where contemporary DIC (DIC_{CO}^{mod}) includes climate variability, climate change and increasing anthropogenic CO_2 with the model drift removed. Anthropogenic DIC (DIC_{AN}^{mod}) includes increasing anthropogenic CO_2, without climate variability or climate change, with the model drift removed. Climate DIC (DIC_{CL}^{mod}) includes climate variability and climate change, without anthropogenic CO_2, with the model drift removed.

The NEMO-PlankTOM12 three-member ensemble mean is within the GCB multi-model range for its representation of the contemporary and anthropogenic CO_2 signals (Figures 1a and 1b), but it has a stronger climate signal compared to the other models for the period 1960–1985 (Figure 1c). This stronger signal is due to the specifics of the spin up combined with the use of NCEP forcing, which is known for its strong trend in Southern Ocean winds. GCB models use a mixture of NCEP, JRA, and ERA forcing fields (Friedlingstein et al., 2021). After 1985, and throughout the period focused on in this study, the climate ensemble is within the GCB multi-model standard deviation (Figure 1c).

2.1.3. Forcing Simulations

Two additional NEMO-PlankTOM12 simulations were carried out to isolate the influence of wind stress on ocean circulation and the influence of wind speed on air-sea gas exchange from the overall climate influence (Table 1; sim^4 and sim^5).

$$DIC_{WSP}^{mod} = sim^3 - sim^4 \quad (4)$$

$$DIC_{WST}^{mod} = sim^3 - sim^5 \quad (5)$$

The remaining effect of buoyancy forcing was then calculated using these two simulations.

$$DIC_{BUO}^{mod} = DIC_{CL}^{mod} - \left(DIC_{WSP}^{mod} + DIC_{WST}^{mod}\right) \quad (6)$$

Buoyancy, therefore, accounts for the remaining climate forcing not included in wind speed or wind stress, including air temperature, humidity, cloud cover, precipitation, and surface pressure.

2.2. Observational Data

The contribution of growing atmospheric CO_2 and climate change and variability can be isolated due to the growing number and quality of ocean observations. The GLODAP database (Olsen et al., 2020) provides DIC observations for the Southern Ocean, quality controlled, back to the 1970s. For the first two decades, data were sparse in both space and time and substantial biases in these data have been identified. During the 1990s, coverage and consistency of data greatly increased, and these improvements continued over subsequent decades (Olsen et al., 2020). Changes in DIC for the contemporary, anthropogenic and climate effects on carbon are calculated using GLODAP observations of DIC and nitrate (GLODAPv2.2020, Olsen et al., 2020), and neural network-based climatology, centered in 1995, of DIC (NNGv2, Broullón et al., 2020) and nitrate (CANYON-B, Bittig et al., 2018; Broullón et al., 2019).

The GLODAP merged master files for DIC and nitrate were gridded onto the NEMO-PlankTOM12 model grid with 31 vertical z levels and into monthly means. The two climatologies were gridded onto the NEMO-PlankTOM12 model grid. The climatologies were then subsampled to GLODAP. The GLODAP database undergoes extensive and systematic quality control and bias checks (Olsen et al., 2020); therefore, no further exclusion of data was carried out.

2.3. Observational Change in DIC

The changes in DIC for the period 1998 to 2018 are calculated for the three carbon types (Contemporary, and its component parts of Anthropogenic and Climate) for both observations and the model. The observed Contemporary change in DIC (ΔDIC^{obs}_{CO}) is calculated as follows:

$$\Delta DIC^{obs}_{CO} = DIC^{obs}_{CO} - DIC^{obs}_{clim} \quad (7)$$

Where DIC^{obs}_{CO} is GLODAPv2.2020 gridded DIC observations averaged from January 1998 to April 2018, and DIC^{obs}_{clim} is the annual average of a climatology of DIC centered on 1995 (Broullón et al., 2020). ΔDIC^{obs}_{CO} is then averaged as a function of latitude. This 1998–2018 time period was selected because (a) it begins after the assumed 5-year climatology of 1995, (b) it includes the most recent observations available in the Southern Ocean for this GLODAP update, (c) it begins in the period when data coverage greatly increased and required data adjustments decreased (Olsen et al., 2020), and (d) it covers a long enough period to remove interannual and reduce interdecadal variability to uncover long-term trends.

We use nitrate to partition the observed contemporary DIC into its component parts of anthropogenic and climate carbon. Nitrate can be used to derive climate influences on DIC, through its fixed ratio with carbon, as its concentration is dominated by dynamic changes in water masses, and less influenced by temperature than oxygen (Bronselaer et al., 2020). The availability of co-located DIC and nitrate observations through GLODAP enhances the value of this method. Observed changes in Anthropogenic (ΔDIC^{obs}_{AN}) and Climate (ΔDIC^{obs}_{CL}) carbon are estimated following the method in Bronselaer et al. (2020);

$$\Delta DIC^{obs}_{AN} = \Delta DIC^{obs}_{CO} - \Delta DIC^{obs}_{CL} \quad (8)$$

$$\Delta DIC^{obs}_{CL} = \frac{117}{16} \times \Delta NO^{obs}_{CO} \quad (9)$$

Where 117/16 is the Redfield Ratio between carbon and nitrogen, multiplied by the change in Contemporary nitrogen (ΔNO^{obs}_{CO});

$$\Delta NO^{obs}_{CO} = NO^{obs}_{CO} - NO^{obs}_{clim} \quad (10)$$

Where NO^{obs}_{CO} is GLODAPv2.2020 nitrate observations, co-located with the DIC observations, from January 1998 to April 2018, and NO^{obs}_{clim} is a climatology of nitrate centered on 1995 (Broullón et al., 2019).

We quantify the GLODAPv2.2020 data set observational uncertainty by adapting the method from Bronselaer et al. (2020). Data set uncertainty is separated into the random error and the observed variability.

$$\sigma^2 = \sqrt{\frac{\sigma^2_{random}}{n} + \sigma^2_{variability}} \quad (11)$$

The random error (random) given for the data set after error correction is described as being consistent to better than 4 μmol/kg (Olsen et al., 2020). This is divided by the number of data points used for the shown mean (n). This data set error is added in quadrature to the uncertainty due to natural variability (variability), taken as the standard deviation of the shown mean, along the time, latitude and longitude axes.

2.4. Model Change in DIC

The modeled change in DIC (ΔDIC^{mod}_{C}) is calculated;

$$\Delta DIC^{mod}_{C} = DIC^{mod}_{C} - DIC^{mod}_{climC} \quad (12)$$

Where C is substituted for each carbon type (CO, AN, CL from Equations 4–6), DIC^{mod} is the NEMO-PlankTOM12 simulation for the relevant carbon type from January 1998 to April 2018 and DIC^{mod}_{clim} is a climatology of the NEMO-PlankTOM12 simulation for the relevant carbon type using January 1993 to December 1997.

The NEMO-PlankTOM12 change in DIC is given both as the full model output, and as the model output subsampled to GLODAPv2.2020 observational coverage spatially and temporally. The similarity between the full and

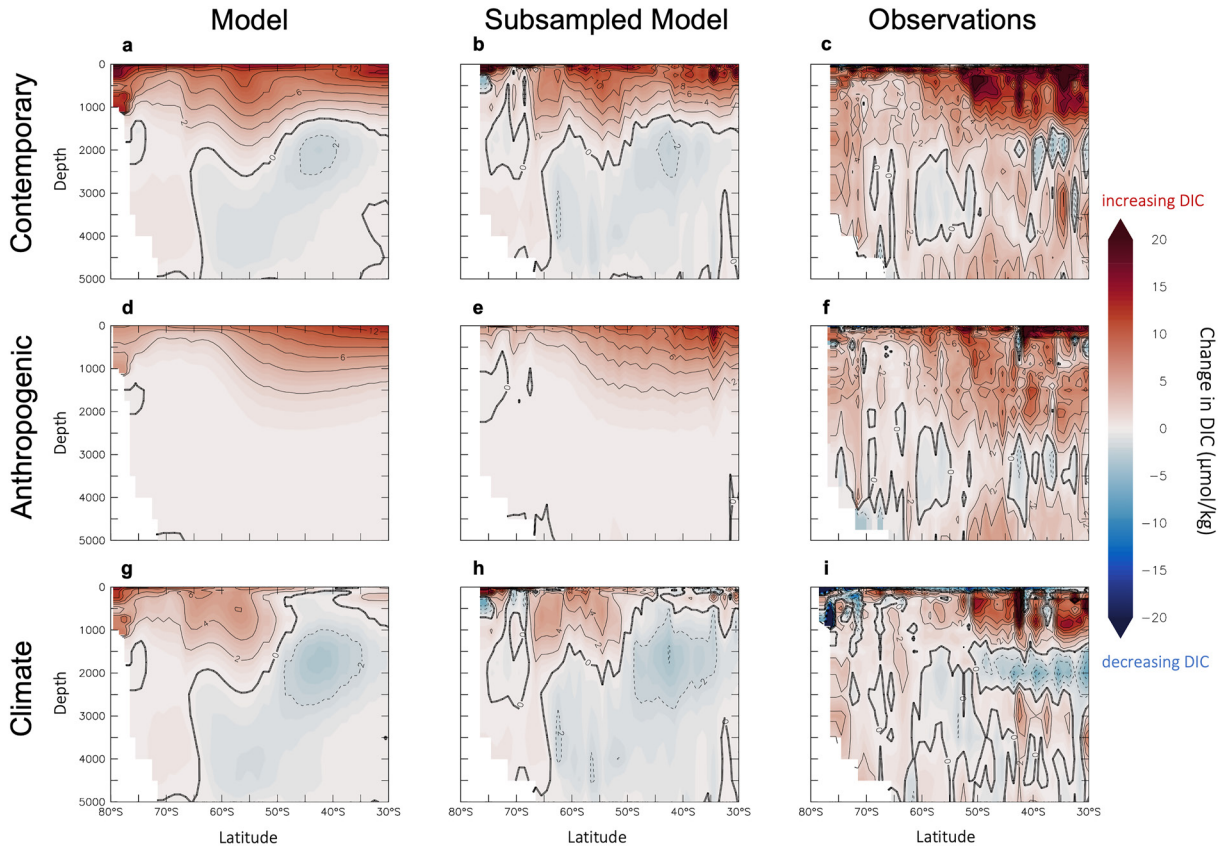

Figure 2. Zonally averaged change in dissolved inorganic carbon (DIC) in the Southern Ocean, for 1998–2018 minus 1995 (µmol/kg). The change in contemporary DIC (a–c) is partitioned into the direct contribution of anthropogenic CO_2 (d–f) and the contribution of climate variability and climate change (g–i). Estimates are based on the NEMO-PlankTOM12 model ensemble (a, d, and g), on the NEMO-PlankTOM12 model ensemble subsampled to the Global Ocean Data Analysis Project (GLODAP) observations (b, e, and h), and on the GLODAP observational data (c, f, and i).

subsampled model ensemble fingerprints provides evidence that the observations are not substantially biased by patchy data collection (Figure 2). A unit conversion is carried out on the model output from µmol/L to µmol/kg to match the observational units. The conversion is carried out using in situ density, temperature, and salinity from the model output.

3. Results

3.1. Detection of a Southern Ocean Climate Fingerprint

At 300–600 m, observations show that both anthropogenic CO_2 and climatic drivers act to increase DIC concentration, with the strength of the signal for both increasing at higher latitudes (North of 55°S; Figure 2). At 2,000 m, climatic drivers act to decrease the DIC concentration, opposing the influence of increasing anthropogenic CO_2, with a stronger decrease at higher latitudes (North of 55°S). These patterns result in a climate fingerprint specific to Southern Ocean change and were detectable in both the observations and the model (Figure 2). The fingerprint of climate dynamics is apparent in the negative DIC at 2,000 m, which indicates the ventilation of natural carbon via transport out of deep water in the upper cell, where it is either upwelled into the mixed layer and outgassed or subducted into the mode and intermediate water to the north, where it reinforces the anthropogenic carbon signal (Figure 2).

In the recent past, the signature of climate variability and climate change is as large as that of anthropogenic CO_2 (Figure 3). Over the period analyzed here, the observations suggest that the natural carbon in the Southern Ocean has changed in a way that limits the absorption of further atmospheric carbon due to a change in the sea-air gradient in pCO_2. For the contemporary signal, the model and observations show a similar magnitude of change both at 300–600 m and at 2,000 m. For the anthropogenic signal, the model is similar to the observations at 300–600 m,

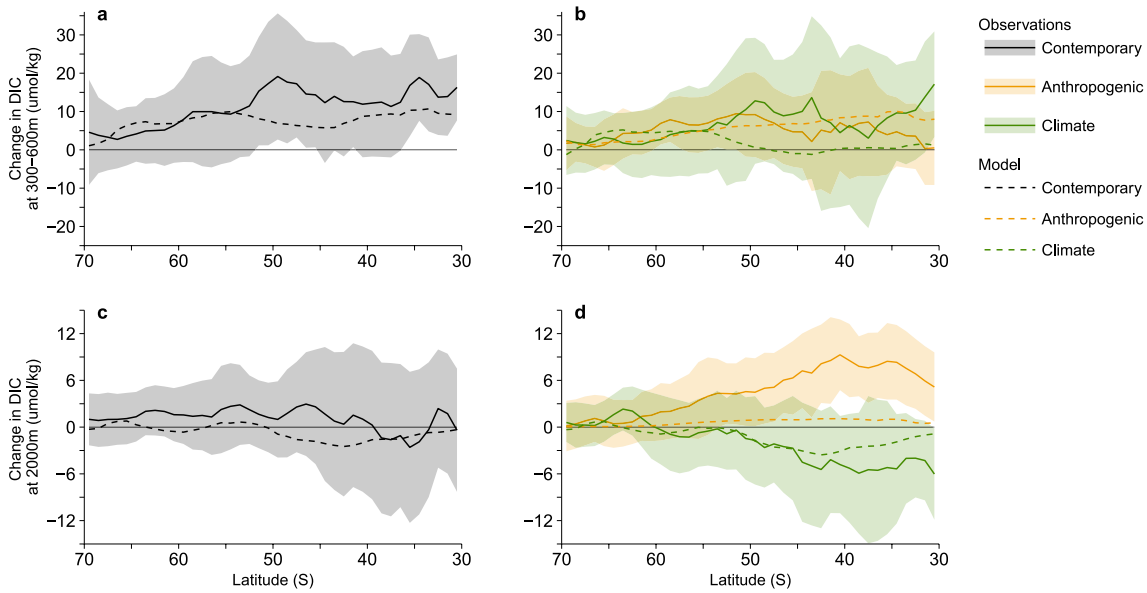

Figure 3. Zonally averaged change in dissolved inorganic carbon (DIC) in the Southern Ocean, for 1998–2018 minus 1995 (μmol/kg). The change in DIC is separated into two depth slices averaged over (a, b) 300–600 and at (c, d) 2,000 m. The change in contemporary DIC (a, c) is partitioned into the direct contribution of anthropogenic CO_2 and the contribution of climate variability and climate change (b, d). Solid lines show the mean and shading shows the error (see method for details) for observations, dashed lines show the mean for the subsampled NEMO-PlankTOM12 model ensemble. A depth slice of 300–600 m is used as it is below strong seasonal influence, helping to reduce noise from seasonal variability. A depth slice of 2,000 m was used as the depth level with the strongest observed climate signal. The gridded data represent a depth thickness of 375 m for both these depths.

while underestimating the signal at 2,000 m. For the climate signal, the model underestimates the observations at 300–600 m, while showing a similar magnitude of change at 2,000 m (Figure 3). The observed climate signal at 2,000 m is distinct from the anthropogenic signal but it is not distinct from zero (Figure 3).

The modeled climate fingerprint of increasing DIC at 300–600 m and decreasing DIC at 2,000 m at higher latitudes (North of 55°S) is detectable across the three ocean basins, with spatial variability in the signal strength (Figure 4). The modeled climate change in the DIC signal shows hotspots in the Pacific basin and south-east Indian basin, consistent with upwelling in regions of intense mode and intermediate water formation (Downes et al., 2017) (Figure 4). Zonal variations in upwelling strength, mixed-layer depth, and mode and intermediate water formation drive the zonal variation in the change in DIC (Downes et al., 2017; Gruber, Landschützer, & Lovenduski, 2019; Morrison et al., 2021; Sallée et al., 2010).

The model underestimates the positive influence of climatic drivers at 300–600 m at lower latitudes (<55°S), leading to a general underestimation of contemporary carbon increase at this depth compared to observations (Figure 3). Despite this underestimation, the model also produces a pattern associated with the upper limb of the overturning circulation and the northward transport of anthropogenic CO_2 and its storage in mode and intermediate water masses (Gruber, Landschützer, & Lovenduski, 2019), with the relatively shallow anthropogenic carbon penetration at higher latitudes and deeper penetration at lower latitudes (<55°S, Figure 2). The model analysis shows that the fingerprint in the observations is unlikely to be due to sampling bias as subsampling the model to the observations does not change the fingerprint pattern (Figure 2). The fingerprint is also unlikely to be due to the summer sampling bias in Southern Ocean observations (Olsen et al., 2020) as the fingerprint persisted when the observed changes were separated into seasons (not shown here).

3.2. Contribution of Natural Climate Drivers to the Climate Fingerprint

Overturning in the Upper Cell transports old water containing natural carbon from the subsurface to the surface via upwelling, where it is outgassed or transported northward and subducted, mixing with anthropogenic carbon uptake from the atmosphere and forming mode and intermediate waters as it crosses the base of the mixed layer. The maximum mixed layer depth (MLD) occurs in winter due to enhanced wind-driven mixing and buoyancy loss (Patara et al., 2021; Sallée et al., 2010). Seasonal re-stratification in spring shallows the MLD, isolating

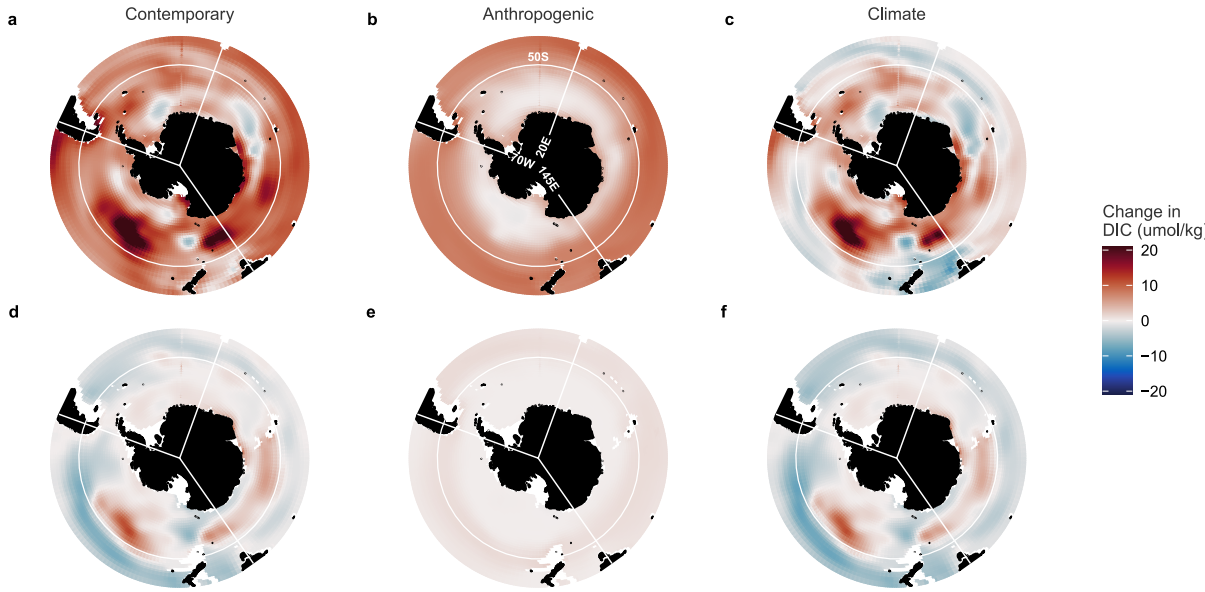

Figure 4. Modeled change in dissolved inorganic carbon (DIC) in the Southern Ocean, for 1998–2018 minus 1995 (μmol/kg). The NEMO-PlankTOM12 ensemble change in DIC is separated into two depth slices averaged over (a–c) 300–600 and (d–f) 2,000 m. The change in the contemporary DIC (a, d) is partitioned into the direct contribution of anthropogenic CO_2 (b, e) and the contribution of climate variability and climate change (c, f). A depth slice of 300–600 m is used as it is below strong seasonal influence, helping to reduce noise from seasonal variability. A depth slice of 2,000 m was used as the depth level with the strongest observed climate signal. The gridded data represent a depth thickness of 375 m for both these depths. Longitude lines show the boundaries of ocean basins.

waters at the bottom of the winter mixed layer from the atmosphere, forming mode and intermediate waters. Biological export production has also been shown to play a role in the transport of carbon through repackaging processes (Gruber, Landschützer, & Lovenduski, 2019; MacGilchrist et al., 2019).

Without the contribution of the climate signal on DIC, the change in contemporary DIC at 300–600 m would be reduced by a factor of almost two north of 55°S, and the change in contemporary DIC at 2,000 m would be increased by a factor of almost two (Figure 3). The effect of climate change and variability on DIC, therefore, has a substantial contribution to the gradient across depths in contemporary carbon, limiting the absorption of further atmospheric carbon due to a change in the sea-air gradient in pCO_2. Within the model, we use this DIC fingerprint to assess the contribution of natural drivers to the climate fingerprint.

We conduct additional model simulations to separate the climate signal into the contribution of wind speed on air-sea CO_2 gas exchange, the effect of wind stress on ocean circulation and the effect of buoyancy fluxes (driven by air temperature, humidity, cloud cover, precipitation and surface pressure; see Section 2.1.3 and Table 1). Wind stress acts to increase DIC south of 50°S and decrease DIC north of 50°S, both at 300–600 m and at 2,000 m (Figure 5). The strongest increase occurs between 55° and 65°S at 300–600 m, while the strongest decrease occurs between 40° and 45°S at 2,000 m. The effects of wind stress on ocean circulation include the vertical and horizontal transport of water through changes in upwelling as well as surface dynamical changes through wind-driven mixing.

The effects of wind speed and buoyancy are small compared to those from wind stress (Figure 5). At 300–600 m, south of 50°S, wind speed and buoyancy act in opposition and mostly cancel each other out, while north of 50°S they both increase DIC by around 1 μmol/kg (Figure 5a). At 2,000 m, south of 50°S, the wind speed effect is close to zero and the buoyancy effect is small, between 0 and −1 μmol/kg. At 2,000 m, north of 50°S, wind speed and buoyancy act in opposition and mostly cancel each other out (Figure 5b). The climate DIC fingerprint is dominated by the effect of wind stress on ocean circulation (Figure 5), especially in the regions where wind speed and buoyancy act in opposition, at 300–600 m south of 50°S (Figure 5a) and at 2,000 m north of 50°S (Figure 5b).

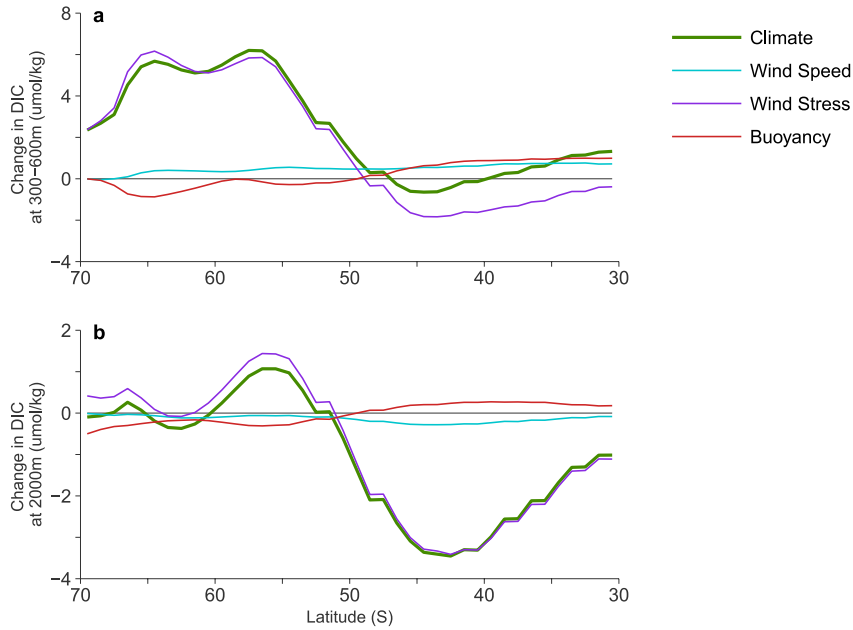

Figure 5. Zonally averaged modeled change in dissolved inorganic carbon (DIC) in the Southern Ocean, for 1998–2018 minus 1995 (μmol/kg). The NEMO-PlankTOM12 ensemble change in DIC is separated into two depth slices averaged over (a) 300–600 and (b) 2,000 m. The change in climate DIC is partitioned into the direct contribution of wind speed (on air-sea CO_2 gas exchange), wind stress (on ocean circulation), and buoyancy fluxes (driven by air temperature, humidity, cloud cover, precipitation, and surface pressure). A depth slice of 300–600 m is used as it is below strong seasonal influence, helping to reduce noise from seasonal variability. A depth slice of 2,000 m was used as the depth level with the strongest observed climate signal. The gridded data represent a depth thickness of 375 m for both these depths.

3.3. Climate Fingerprint Over Time and Implications for the Southern Ocean Carbon Flux

Interdecadal variability in DIC trends is expected, following patterns of saturation and reinvigoration found in studies of surface carbon fluxes (Keppler & Landschützer, 2019; Landschützer et al., 2015; Le Quéré et al., 2007). In Figure 6, the observed climate DIC change is decomposed into 5-year time periods. At 2,000 m, there is minimal change for 1998:2002, followed by a sharp decrease for 2003:2007 down to a mean of −7.3 μmol/kg, with the uncertainty not quite distinct from zero. After this minimum, the DIC at 2,000 m gradually increases over time to −5.9 and −4.6 μmol/kg (Figure 6a). At 300–600 m, the maximum change in DIC is for 1998:2002 with a mean of 12.2 μmol/kg; after this, the DIC decreases to between 4.8 and 7.7 μmol/kg without a clear trend over time (Figure 6a). Over the full period (1998:2018), the observed climate DIC change is 7.0 μmol/kg at 300–600 m and −5.2 μmol/kg at 2,000 m (Figure 6b).

The upwelling of natural carbon limits the amount of atmospheric CO_2 that the ocean can absorb. This mechanism in the Southern Ocean is already well documented and understood (Gruber, Landschützer, & Lovenduski, 2019; Lenton et al., 2013); our work (Figure 6) indicates that this mechanism may have increased over recent decades, with implications for the future strength of the Southern Ocean carbon flux, if this fingerprint persists. Following the logic of enhanced upwelling bringing more climate carbon from depth to surface waters, the saturation period (pre-2002) (Landschützer et al., 2015; Le Quéré et al., 2007) can be assumed to coincide with an increase in climate DIC at the surface (and smaller negative change in DIC at depth), so high climate carbon in surface waters reduces the sea-air difference in carbon, reducing the uptake of atmospheric CO_2. An increase in the climate change in DIC at 300–600 m and a small change in DIC at 2,000 m are shown in the observations here for the period 1998:2002 (Figure 6). The reinvigoration period (2003–2012) (Landschützer et al., 2015) can then be assumed to coincide with a decrease in climate DIC at 300–600 m (and larger negative change at 2,000 m), so low climate carbon in surface waters increases the sea-air difference in carbon, increasing the uptake of atmospheric CO_2. This decrease in climate DIC change at 300–600 m and larger negative change at 2,000 m for the period 2003:2012 can also be detected here in the observations (Figure 6).

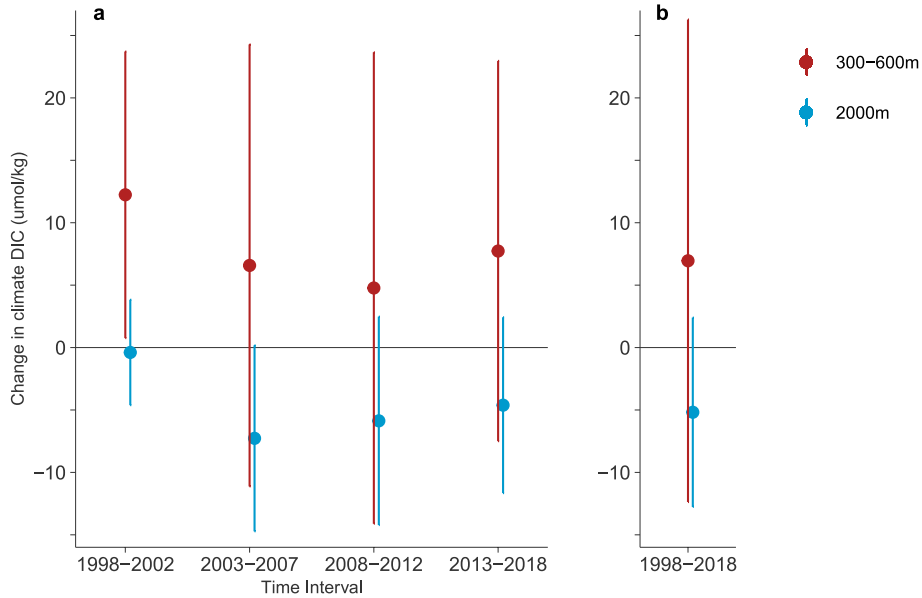

Figure 6. Zonally averaged observed change in climate dissolved inorganic carbon (DIC) in the Southern Ocean for 1998–2018 minus 1995 (μmol/kg). The change in climate DIC is averaged over 43°–33°S and separated into two depth slices averaged over (a–c) 300–600 m and (d–f) 2,000 m. The change in climate DIC is shown as 5-year time intervals (a) and over the full period (b). Circles show the mean and error bars show the error (instrumental error and natural variability over time, longitude, latitude, and depth, see method for details). A depth slice of 300–600 m is used as it is below strong seasonal influence, helping to reduce noise from seasonal variability. A depth slice of 2,000 m was used as the depth level with the strongest observed climate signal. The gridded data represent a depth thickness of 375 m for both these depths.

4. Discussion

Using a combined analysis of observations and a model, we showed that the impact of climate change and variability on DIC is as large as the impact of changing atmospheric CO_2 concentration in the Southern Ocean over the period 1998–2018. This signal is specific to the Southern Ocean because of the unique combination of highly variable winds, strong upwelling, and subduction and northward transport of the surface DIC. This unique property means that the Southern Ocean is an ideal location to detect the fingerprint of climate change on the DIC.

Our model analysis suggests that strong winds lead to a specific fingerprint with enhanced DIC at 300–600 m and decreased DIC at 2,000 m, which is driven by changes in upwelling. Such a fingerprint is also detected in the observations with the DIC signals at 300–600 and 2,000 m distinct from each other. However, the 2,000 m signal is not distinct from zero in the observed estimate, and the modeled climate signal is larger than other similar models. Therefore, a firm attribution cannot yet be done. If the signal is indeed caused by increasing winds, and the winds continue to increase from the combination of slow ozone recovery and continued global warming, the fingerprint should emerge distinctly from zero in the future. The collection of in situ nitrate data in addition to DIC at a depth of around 2,000 m between 50° and 30°S is identified here as a key to track climate-driven changes in carbon in the Southern Ocean.

The sparsity of observations in the Southern Ocean is a shortcoming to any investigation of this kind, potentially biasing results to certain regions, years and seasons. We have tried to limit the impact of this shortcoming in several ways, including looking at the period after 1995 when data coverage in the Southern Ocean greatly increased (Olsen et al., 2020), subsampling the climatology to the observations, quantifying an observational error (Section 2.3), and comparing the model fingerprint to the subsampled model fingerprint (Section 2.4 and Figure 2).

Our results concur with a recent review of carbon in the Southern Ocean that highlights that while there are several published estimates of changes in anthropogenic carbon, there is no equivalent for changes in climate carbon (Gruber, Landschützer, & Lovenduski, 2019). Our analysis of the GLODAP observations concurs with the periods of "saturation" (Le Quéré et al., 2007) and "reinvigoration" (Landschützer et al., 2015) of the

Southern Ocean carbon sink, adding to the evidence of the mechanisms driving these shifting trends. DeVries et al. (2017) show how changes in the upper ocean (0–1,000 m) overturning circulation for the 1980s to the 2000s may have affected climate and anthropogenic carbon fluxes, with weakening overturning in the 2000s reducing outgassing of natural CO_2 and increasing the uptake of anthropogenic CO_2, thus increasing the total carbon flux. Our findings agree with this mechanism and highlight that stronger overturning (associated with stronger winds) decreases the carbon flux from the atmosphere to the ocean. McKinley et al. (2020) attribute the variability of the global sink to external forcing, namely the variable growth rate of atmospheric CO_2, where the slowed growth rate of atmospheric CO_2 results in a slowed ocean carbon sink. In contrast, our findings suggest that the effect of climate variability and climate change on CO_2 fluxes is nearly as large as that of rising atmospheric CO_2 in the Southern Ocean over the last decades, with most of the variability coming from climate effects.

Our findings differ from those of Bronselaer et al. (2020). In their study, the climate (dynamic) DIC change increases more in the surface south of 60°S, while here we find the change in DIC increases more in the surface north of 60°S compared to the south. Our other findings cannot be compared as they only looked above 2,000 m, and only found significance much shallower from around 500 m. They found that wind-driven mixing and meltwater effects (within buoyancy here) reinforce each other in the surface south of 60°S (Bronselaer et al., 2020), while we find that for the same region buoyancy counteracts wind-driven mixing. The key reasons behind these differences include; the change in DIC being calculated with a time period of 2014:2019 minus 1985:2005; different observational datasets (SOCCOM for later period and GLODAP ship-board for earlier period), and in our study buoyancy is driven by air temperature, humidity, cloud cover, precipitation, and surface pressure, while they look at meltwater effects specifically (Bronselaer et al., 2020). These differences in model setup, observations and time periods likely account for much of the difference between findings.

Model improvements could include a higher resolution allowing for meso-scale eddy parameterization to compare with the current eddy resolving model, testing different ice models to see if there is a change in the wind/buoyancy relationship around the Antarctic coastline, and testing different wind forcing products to determine if they affect both the strength and the timing of the climate fingerprint. The next steps for this work could also include updating the change in DIC with new GLODAP releases to extend the time period, and testing other methods for separating contemporary carbon into anthropogenic and climate, that is, the eMLR(C*) method, which uses observed alkalinity and phosphate along with extended multiple linear regression (Clement & Gruber, 2018). Both the eMLR(C*) method and the method used in this study utilize biogeochemical observations other than DIC to separate contemporary carbon, each with different benefits and drawbacks.

5. Conclusion

We identify a distinct climate fingerprint in the observed Southern Ocean DIC. Our model analysis suggests that this contemporary DIC fingerprint can be explained by a combination of anthropogenic carbon ventilation of waters at 300–600 m, and climate carbon redistribution from waters at 2,000 m to waters at 300–600 m, reducing climate carbon at 2,000 m while enhancing it at 300–600 m. Observations over a longer time period, and models with more complete processes, will be needed before confirming the presence of trend. We show here that measurements that keep track of this distinct fingerprint may facilitate the early detection of climate-driven trends in DIC reorganization in the Southern Ocean interior.

Conflict of Interest

The authors declare no conflicts of interest relevant to this study.

Data Availability Statement

The data that support the findings of this study are published openly at GLODAP (https://www.glodap.info/). The NEMO-PlankTOM12 simulations used in this study are available on request from the lead author.

Acknowledgments
R.M.W. and N.M. were funded by the UK Natural Environment Research Council (SONATA: Grant NE/P021417/1). N.M. also received funding from the European Commission EC H2020 (4C; Grant 821003). C.L.Q. was funded by the UK Royal Society (Grant RP\R1\191063). AO appreciates funding from the EU H2020 project COMFORT (Grant 820989). Thanks to Erik Buitenhuis and David Willis for their work on the NEMO-PlankTOM12 model development. Thanks to the many scientists involved in all stages of producing the invaluable GLODAP database. The research presented in this paper was carried out on the High Performance Computing Cluster supported by the Research and Specialist Computing Support service at the University of East Anglia.

References

Bittig, H. C., Steinhoff, T., Claustre, H., Fiedler, B., Williams, N. L., Sauzède, R., et al. (2018). An alternative to static climatologies: Robust estimation of open ocean CO_2 variables and nutrient concentrations from T, S, and O_2 data using Bayesian neural networks. *Frontiers in Marine Science*, *5*, 328. https://doi.org/10.3389/fmars.2018.00328

Bronselaer, B., Russell, J. L., Winton, M., Williams, N. L., Key, R. M., Dunne, J. P., et al. (2020). Importance of wind and meltwater for observed chemical and physical changes in the Southern Ocean. *Nature Geoscience*, *13*(1), 35–42. https://doi.org/10.1038/s41561-019-0502-8

Broullón, D., Pérez, F. F., Velo, A., Hoppema, M., Olsen, A., Takahashi, T., et al. (2019). A global monthly climatology of total alkalinity: A neural network approach. *Earth System Science Data*, *11*(3), 1109–1127. https://doi.org/10.5194/essd-11-1109-2019

Broullón, D., Pérez, F. F., Velo, A., Hoppema, M., Olsen, A., Takahashi, T., et al. (2020). A global monthly climatology of oceanic total dissolved inorganic carbon: A neural network approach. *Earth System Science Data*, *12*(3), 1725–1743. https://doi.org/10.5194/essd-12-1725-2020

Buitenhuis, E. T., Hashioka, T., & Le Quéré, C. (2013). Combined constraints on global ocean primary production using observations and models. *Global Biogeochemical Cycles*, *27*(3), 847–858. https://doi.org/10.1002/gbc.20074

Clement, D., & Gruber, N. (2018). The eMLR(C*) method to determine decadal changes in the global ocean storage of anthropogenic CO_2. *Global Biogeochemical Cycles*, *32*(4), 654–679. https://doi.org/10.1002/2017GB005819

DeVries, T., Holzer, M., & Primeau, F. (2017). Recent increase in oceanic carbon uptake driven by weaker upper-ocean overturning. *Nature*, *542*(7640), 215–218. https://doi.org/10.1038/nature21068

DeVries, T., Le Quéré, C., Andrews, O., Berthet, S., Hauck, J., Ilyina, T., et al. (2019). Decadal trends in the ocean carbon sink. *Proceedings of the National Academy of Sciences of the United States of America*, *116*(24), 201900371–11651. https://doi.org/10.1073/pnas.1900371116

Downes, S. M., Langlais, C., Brook, J. P., & Spence, P. (2017). Regional impacts of the westerly winds on Southern Ocean mode and intermediate water subduction. *Journal of Physical Oceanography*, *47*(10), 2521–2530. https://doi.org/10.1175/JPO-D-17-0106.1

Fox-Kemper, B., Hewitt, H. T., Xiao, C., Aðalgeirsdóttir, G., Drijfhout, S. S., Edwards, T. L., et al. (2021). Ocean, cryosphere and sea level change. Climate change 2021: The physical 12 science basis. Contribution of working group I to the sixth assessment report of the intergovernmental 13 Panel on climate change.

Friedlingstein, P., Jones, M. W., O'Sullivan, M., Andrew, R. M., Bakker, D. C. E., Hauck, J., et al. (2021). Global carbon budget 2021. *Earth System Science Data Discussions*, 1–191. https://doi.org/10.5194/essd-2021-386

Fyfe, J. C., & Saenko, O. A. (2006). Simulated changes in the extratropical Southern Hemisphere winds and currents. *Geophysical Research Letters*, *33*(6), L06701. https://doi.org/10.1029/2005GL025332

Gloege, L., McKinley, G. A., Landschützer, P., Fay, A. R., Frölicher, T. L., Fyfe, J. C., et al. (2021). Quantifying errors in observationally based estimates of ocean Carbon sink variability. *Global Biogeochemical Cycles*, *35*(4), e2020GB006788. https://doi.org/10.1029/2020GB006788

Gruber, N., Clement, D., Carter, B. R., Feely, R. A., van Heuven, S., Hoppema, M., et al. (2019). The oceanic sink for anthropogenic CO_2 from 1994 to 2007. *Science*, *363*(6432), 1193–1199. https://doi.org/10.1126/science.aau5153

Gruber, N., Landschützer, P., & Lovenduski, N. S. (2019). The variable Southern Ocean carbon sink. *Annual Review of Marine Science*, *11*(1), 159–186. https://doi.org/10.1146/annurev-marine-121916-063407

Hauck, J., Zeising, M., Le Quéré, C., Gruber, N., Bakker, D. C. E., Bopp, L., et al. (2020). Consistency and challenges in the ocean carbon sink estimate for the global carbon budget. *Frontiers in Marine Science*, *7*, 571720. https://doi.org/10.3389/fmars.2020.571720

Keppler, L., & Landschützer, P. (2019). Regional wind variability modulates the southern Ocean Carbon sink. *Scientific Reports*, *9*(1), 7384. https://doi.org/10.1038/s41598-019-43826-y

Landschützer, P., Gruber, N., Haumann, F. A., Rödenbeck, C., Bakker, D. C. E., Van Heuven, S., et al. (2015). The reinvigoration of the Southern Ocean carbon sink. *Science*, *349*(6253), 1221–1224. https://doi.org/10.1126/science.aab2620

Lenton, A., Tilbrook, B., Law, R. M., Bakker, D., Doney, S. C., Gruber, N., et al. (2013). Sea–air CO_2 fluxes in the Southern Ocean for the period 1990–2009. *Biogeosciences*, *10*(6), 4037–4054. https://doi.org/10.5194/bg-10-4037-2013

Le Quéré, C., Buitenhuis, E. T., Moriarty, R., Alvain, S., Aumont, O., Bopp, L., et al. (2016). Role of zooplankton dynamics for Southern Ocean phytoplankton biomass and global biogeochemical cycles. *Biogeosciences*, *12*(14), 11935–11985. https://doi.org/10.5194/bgd-12-11935-2015

Le Quéré, C., Rödenbeck, C., Buitenhuis, E. T., Conway, T. J., Langenfelds, R., Gomez, A., et al. (2007). Saturation of the southern Ocean CO_2 sink due to recent climate change. *Science*, *316*(5832), 1735–1738. https://doi.org/10.1126/science.1136188

MacGilchrist, G. A., Naveira Garabato, A. C., Brown, P. J., Jullion, L., Bacon, S., Bakker, D. C. E., et al. (2019). Reframing the carbon cycle of the subpolar Southern Ocean. *Science Advances*, *5*(8), 1–9. https://doi.org/10.1126/sciadv.aav6410

Madec, G. (2013). *NEMO ocean engine* (Vol. 27). Note Du Pole de Modélisation de Institut Pierre-Simon Laplace (IPSL). https://doi.org/10.5281/zenodo.1464817

McKinley, G. A., Fay, A. R., Eddebbar, Y. A., Gloege, L., & Lovenduski, N. S. (2020). External forcing explains recent decadal variability of the Ocean Carbon sink. *AGU Advances*, *1*(2), e2019AV000149. https://doi.org/10.1029/2019AV000149

Meredith, M., Sommerkorn, M., Cassotta, S., Derksen, C., Ekaykin, A., Hollowed, A., et al. (2019). Polar regions. In H. O. Pörtner, D. C. Roberts, V. Masson-Delmotte, P. Zhai, M. Tignor, E. Poloczanska, et al. (Eds.), *IPCC special report on the Ocean and crysphere in a changing climate*.

Morrison, A. K., Waugh, D. W., Hogg, A. M., Jones, D. C., & Abernathey, R. P. (2021). Ventilation of the Southern Ocean pycnocline. *Ventilation of the Southern Ocean Pycnocline*, *26*(1), 405–430. https://doi.org/10.1146/annurev-marine-010419-011012

Olsen, A., Lange, N., Key, R. M., Tanhua, T., Bittig, H. C., Kozyr, A., et al. (2020). GLODAPv2.2020 – The second update of GLODAPv2. (preprint). *Oceanography – Chemical*. https://doi.org/10.5194/essd-2020-165

Patara, L., Böning, C. W., & Tanhua, T. (2021). Multidecadal changes in Southern Ocean ventilation since the 1960s driven by wind and buoyancy forcing. *Journal of Climate*, *34*(4), 1485–1502. https://doi.org/10.1175/JCLI-D-19-0947.1

Sallée, J. B., Speer, K. G., & Rintoul, S. R. (2010). Zonally asymmetric response of the Southern Ocean mixed-layer depth to the southern annular mode. *Nature Geoscience*, *3*(4), 273–279. https://doi.org/10.1038/ngeo812

Thompson, D. W. J., & Solomon, S. (2002). Interpretation of recent southern hemisphere climate change. *Science*, *296*(5569), 895–899. https://doi.org/10.1126/science.1069270

Thompson, D. W. J., Solomon, S., Kushner, P. J., England, M. H., Grise, K. M., & Karoly, D. J. (2011). Signatures of the Antarctic ozone hole in Southern Hemisphere surface climate change. *Nature Geoscience*, *4*(11), 741–749. https://doi.org/10.1038/ngeo1296

Timmermann, R., Goosse, H., Madec, G., Fichefet, T., Ethe, C., & Duliere, V. (2005). On the representation of high latitude processes in the ORCA-LIM global coupled sea ice–ocean model. *Ocean Modelling*, *8*(1–2), 175–201. https://doi.org/10.1016/j.ocemod.2003.12.009

Wright, R. M., Le Quéré, C., Buitenhuis, E., Pitois, S., & Gibbons, M. J. (2021). Role of jellyfish in the plankton ecosystem revealed using a global ocean biogeochemical model. *Biogeosciences*, *18*(4), 1291–1320. https://doi.org/10.5194/bg-18-1291-2021